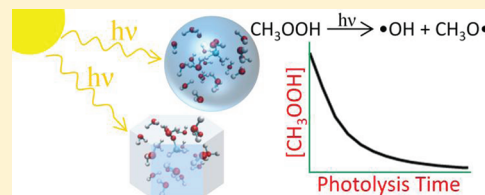


Absorption Spectra and Photolysis of Methyl Peroxide in Liquid and Frozen Water

Scott A. Epstein,[†] Dorit Shemesh,[‡] Van T. Tran,[†] Sergey A. Nizkorodov,^{*,†} and R. Benny Gerber^{*,†,‡}[†]Department of Chemistry, University of California, Irvine, California 92697, United States[‡]Department of Physical Chemistry and the Fritz Haber Research Center for Molecular Dynamics, Hebrew University, Jerusalem 91904, Israel

Supporting Information

ABSTRACT: Methyl peroxide (CH₃OOH) is commonly found in atmospheric waters and ices in significant concentrations. It is the simplest organic peroxide and an important precursor to hydroxyl radical. Many studies have examined the photochemical behavior of gaseous CH₃OOH; however, the photochemistry of liquid and frozen water solutions is poorly understood. We present a series of experiments and theoretical calculations designed to elucidate the photochemical behavior of CH₃OOH dissolved in liquid water and ice over a range of temperatures. The molar extinction coefficients of aqueous CH₃OOH are different from the gas phase, and they do not change upon freezing. Between -12 and 43 °C, the quantum yield of CH₃OOH photolysis is described by the following equation: $\Phi(T) = \exp((-2175 \pm 448)/T) + 7.66 \pm 1.56$. We use on-the-fly ab initio molecular dynamics simulations to model structures and absorption spectra of a bare CH₃OOH molecule and a CH₃OOH molecule immersed inside 20 water molecules at 50, 200, and 220 K. The simulations predict large sensitivity in the absorption spectrum of CH₃OOH to temperature, with the spectrum narrowing and shifting to the blue under cryogenic conditions because of constrained dihedral motion around the O–O bond. The shift in the absorption spectrum is not observed in the experiment when the CH₃OOH solution is frozen suggesting that CH₃OOH remains in a liquid layer between the ice grains. Using the extinction coefficients and photolysis quantum yields obtained in this work, we show that under conditions with low temperatures, in the presence of clouds with a high liquid–water content and large solar zenith angles, the loss of CH₃OOH by aqueous photolysis is responsible for up to 20% of the total loss of CH₃OOH due to photolysis. Gas phase photolysis of CH₃OOH dominates under all other conditions.



INTRODUCTION

Methyl peroxide (CH₃OOH) is the simplest organic peroxide and is a major reservoir of hydroxyl radical.^{1,2} In the atmosphere, CH₃OOH is formed by oxidation of volatile organic compounds such as methane, ethane, isoprene, and α -pinene by OH, O₃, and NO₃.³ It is present in both the polluted^{4–6} and remote troposphere.^{5,7,8} It is also detected in rainwater^{4,9,10} and in snow and ice crystals.¹ In addition, significant organic peroxide concentrations are found in atmospheric particulate matter.^{11,12}

Photolysis of CH₃OOH is an important free-radical generating pathway that occurs in the gas phase, in cloud droplets of aqueous liquid solutions, and in ice crystals. The photophysical properties^{3,13,14} and photochemical behavior^{3,15–17} of gaseous CH₃OOH are well understood. The absorption spectrum of gas phase CH₃OOH is dominated by a dissociative $n \rightarrow \sigma^*$ transition centered below 200 nm. The red shoulder of this transition extends in the atmospherically relevant range (250–400 nm), and accurate absorption cross-sections are available over this entire range.^{3,13,14,18,19} The primary gas phase photolysis pathway is cleavage of the O–O bond forming OH and CH₃O occurring with a quantum yield approaching unity.³ In the presence of oxygen, formaldehyde has been identified as the major end-product of gaseous

CH₃OOH photolysis.^{3,18} Gas phase CH₃OOH is removed from the atmosphere by reaction with OH and photolysis^{20,21} with a typical lifetime of more than a day.^{21,22}

In contrast to the gas phase, the photochemistry of aqueous liquid and frozen solutions of CH₃OOH is far more uncertain. Molina and Arguello¹⁴ and Lederle and Rieche²³ measured extinction coefficients of aqueous CH₃OOH over a limited range of wavelengths. Monod and co-workers²⁰ measured the kinetics and reaction products of CH₃OOH photolysis in liquid water. They saw formation of formaldehyde and lesser amounts of formic acid upon photolysis. Aqueous photolysis quantum yield data are not currently available. Photolysis kinetics can be dependent on the phase of the aqueous solution.²⁴ To the best of our knowledge, photochemistry of CH₃OOH in ice has not been investigated.

The importance of photolysis of aqueous phase CH₃OOH extends beyond this simple molecule. A number of more complicated organic peroxides (ROOH) exist in organic

Special Issue: A. R. Ravishankara Festschrift

Received: November 23, 2011

Revised: December 23, 2011

Published: January 4, 2012

aerosols, and some of them are water soluble.^{12,25} Since photochemistry of large organic molecules is driven by functional groups, we use CH₃OOH as a model compound to elucidate the general kinetic behavior of organic peroxides in the condensed phase. The condensed phase chemistry of these larger ROOH species will be a function of their solubilities and aqueous phase photolysis rates.

Because of the importance of CH₃OOH, its structure and dynamics in water and ice has been studied by several theoretical approaches. Kulkarni et al.²⁶ investigated the possible structures of CH₃OOH with up to 5 water molecules at the MP2/6-31G(d,p) and MP2/6-311++G(2d,2p) levels. Ignatov et al.⁷ used PM3 and DFT(BLYP/6-31++G(d,p)) calculations to model the interaction between CH₃OOH and an ice surface using larger ice clusters. Both studies focused on the interaction energies between the CH₃OOH and the water/ice and the preferred location of the methyl peroxide in the cluster. They concluded that the hydrophobic CH₃ group prefers to dangle outside the cluster. In addition, Ignatov et al. demonstrated that the adsorption of CH₃OOH is heavily favored over its intrusion into the ice surface. They also concluded that the PM3 potential and DFT predict similar binding energies.

Kamboures et al.²⁷ used on-the-fly ab initio dynamics on a semiempirical PM3 potential to study the photodissociation of CH₃OOH adsorbed on 20 water molecules. Following the breakage of the O–O bond, secondary reactions between OH and CH₃O on frozen water clusters were shown to yield formaldehyde, water, hydrogen, carbon monoxide, methanol, hydrogen peroxide, and other products on a picosecond time scale. Geminate recombination of OH and CH₃O was not observed. A key assumption in that study was that relaxation to the ground state is very fast, and therefore, it is sufficient to start the simulation on the ground electronic state with an already elongated O–O bond. The validity of this assumption was later confirmed in a follow-up study by Shemesh and Gerber²⁸ on the same system. The first half picosecond of photochemistry was modeled using a nonadiabatic surface hopping method combined with a semiempirical potential, a considerable improvement over the previous study by Kamboures et al., which constrained the dynamics to the ground electronic state. Shemesh and Gerber evaluated the role of different excited states in the photochemistry, the time scales of photodissociation, and the relaxation to the ground state. The relaxation to the ground state is fast (<20 fs), especially at cryogenic temperatures.

The absorption cross-sections of CH₃OOH in liquid and frozen water are important parameters that have yet to be measured across the range of atmospherically relevant wavelengths and temperatures. In this article, we provide the extinction coefficients that describe the UV absorption of aqueous liquid and frozen methyl peroxide solutions. We also present on-the-fly ab initio molecular dynamic simulations of a bare CH₃OOH molecule, designed to simulate the gas phase, and compare them to simulations of a CH₃OOH molecule immersed inside 20 water molecules at a range of temperatures. These simulations provide new insights into the structure and absorption spectra of CH₃OOH in water and ice.

The photolysis quantum yields are equally important parameters for predicting the photochemical fate of CH₃OOH in aqueous environments. Using a relative rate approach, the UV-photolysis yields of methyl peroxide in liquid water and ice are determined over a range of temperatures.

These are the first photolysis yield measurements of CH₃OOH in liquid and frozen water, which make it possible to evaluate the relative importance of aqueous vs gas phase photochemistry of this peroxide.

■ MATERIALS AND METHODS

Synthesis and Identification of Methyl Peroxide.

Methyl peroxide is not available commercially and, therefore, was synthesized by methylation of hydrogen peroxide as described by Vaghjiani and Ravishankara¹³ with minor modifications. A 12 M solution of KOH (Fisher Scientific >85%) was slowly added to a stirred mixture of hydrogen peroxide (30% Fisher Scientific), dimethyl sulfate (Sigma Aldrich ≥99.8%), and purified water in an ice bath. A reflux column was used to retain the less volatile CH₃OOH product while allowing the more volatile CH₃OOCH₃ byproduct to escape. This mixture was then acidified with sulfuric acid (EMD Chemicals 95%) and extracted into diethyl ether (EMD Chemicals 99%). We added purified water atop the organic phase and carefully boiled off the diethyl ether in a rotary evaporator. An aqueous solution of methyl peroxide with a minimal amount of impurities was produced.

We used ¹H NMR to confirm the purity of the product. ¹H NMR of the solution from the synthesis procedure extracted into deuterated chloroform resulted in two significant non-solvent peaks: 8.20 ppm integrating to 0.9977 and 3.91 ppm integrating to 2.999 (see Supporting Information). The 3:1 ratio of peak integrals conclusively identifies the unknown peroxide as methyl peroxide. The 3:1 ratio rules out the presence of H₂O₂ or CH₃OOCH₃, the most likely impurities from the synthesis procedure.

The concentration of CH₃OOH was quantified with an iodometric peroxide test originally proposed by Banerjee and Budke in 1964²⁹ and frequently used in subsequent publications.^{11,12,25} This test detects visible absorption of I₃⁻ ions formed from the reaction of a water-soluble peroxide with excess I⁻. A calibration curve relating peroxide concentration with I₃⁻ absorbance was constructed using solutions of H₂O₂ with known concentrations. We found that the oxidation of I⁻ by CH₃OOH reactions was considerably slower than the oxidation of I⁻ by H₂O₂. Therefore, we recommend measuring I₃⁻ concentration over a period of 4 h for water-soluble organic peroxides to ensure that the reaction has come to equilibrium (see Supporting Information).

Hazards of Methyl Peroxide Handling. Pure or highly concentrated methyl peroxide is known to be explosive. Caution should be exercised to ensure that methyl peroxide always remains in solution. Concentrations of all aqueous solutions prepared in this work did not exceed 1 M.

Description of Experimental Apparatuses. Two separate experimental setups were needed for UV–vis absorption measurements of methyl peroxide in liquid water (Figure 1A) and in ice (Figure 1B).

The apparatus used for liquid solutions consists of a Shimadzu constant temperature cell holder inside a Shimadzu model 2350 UV–vis spectrometer. The cell holder was modified to hold a 3/8" fiber that delivers actinic UV-radiation (>275 nm, 150 mW) from a 150 W xenon arc lamp housing (Newport model 6256). A quartz cuvette containing a dilute methyl peroxide solution was loaded into the sample compartment. Nanopure water in an identical quartz cuvette was used as a reference. The sample compartment was continuously purged with dry, purified air to prevent water

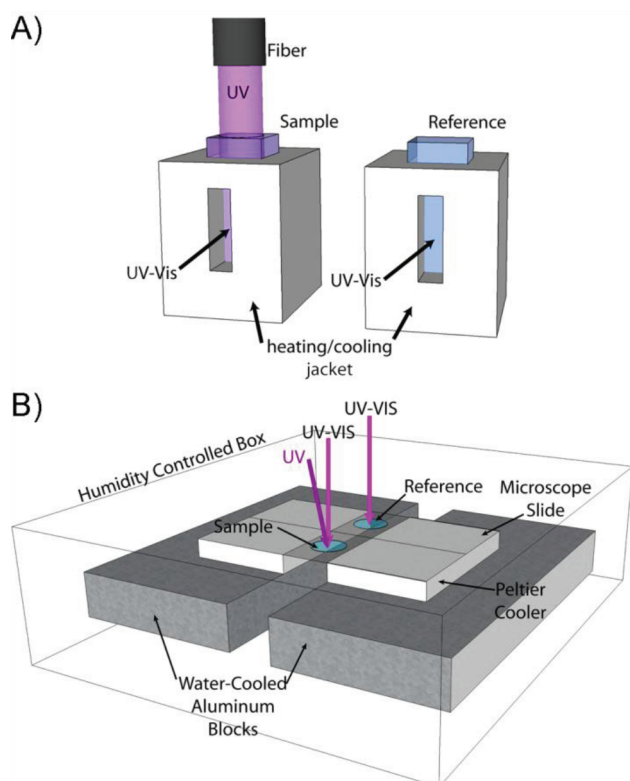


Figure 1. (A) Experimental setup used for photolyzing temperature controlled liquid solutions inside a Shimadzu UV-vis spectrometer. (B) Experimental setup used to photolyze frozen ice films under real-time surveillance with two fiber-optic UV-vis spectrometers.

condensation on the cuvettes for experiments conducted below room temperature. This setup allows for UV-vis absorption measurements and sample photolysis at a prescribed temperature (0–80 °C).

UV-vis absorption measurements of methyl peroxide in ice were more complicated, as the increased complexity and customization of this apparatus reflects (Figure 1B). Absorption measurements were made through a sample and water reference frozen atop two identical quartz microscope slides. A 15 μL drop of sample and pure water were placed on the sample and reference slides, respectively, and covered with quartz coverslips to minimize evaporation and create a more uniform film thickness ($\sim 120 \mu\text{m}$). Ice films were sufficiently thick to make the chemistry dominated by the bulk with a negligible contribution from surface processes. Liquid films were cooled by direct heat withdrawal from the microscope slides, which reached their set temperature between $-5 \text{ }^\circ\text{C}$ and $-15 \text{ }^\circ\text{C}$ at a rate on the order of $0.1 \text{ }^\circ\text{C}$ per second. A representative picture of the sample before and after freezing is presented in the Supporting Information. Slides were cooled by thermal contact with two $50 \times 50 \text{ mm}$ Peltier coolers (Tellurex C2-50-1514) separately controlled by two temperature controllers (TE Technology, Inc. TC-48-20). Each Peltier cooler was in thermal contact with a water-cooled aluminum heat sink.

In order to measure absorption spectra of the liquid or frozen films, light from a deuterium light source (Ocean Optics, DH-2000) was split and sent through the sample and reference and collected in two UV-vis spectrometers (Ocean Optics, USB-4000) with $600 \mu\text{m}$ optical fibers. Photolysis radiation was delivered through a larger fiber from the 150 W xenon arc lamp

housing and projected onto the sample slide under a 15° angle. In order to minimize sample heating, a 330 nm bandpass filter (Edmund Industrial Optics, NT46–438) and a dilute solution of $\text{NiSO}_4 \cdot 6\text{H}_2\text{O}$ ³⁰ were used to filter out visible and infrared light from both photolysis and absorbance measurement light sources. About 50 mW of photolyzing radiation between 275 and 390 nm reached the sample. The power of the absorbance measurement radiation was too small to measure, and it did not contribute to photolysis. An electronic shutter was used for blocking the photolyzing radiation without turning the arc lamp off. The compartment that housed the ice films was continuously purged with dry, purified air to prevent water condensation on the microscope slides and coverslips. The temperature of the ice films was monitored with a type-K thermocouple mounted to the sample microscope slide. The temperature of the ice film remained constant within $0.3 \text{ }^\circ\text{C}$ throughout the entire experiment.

Determining Photolysis Yields. Since we are using a broadband excitation source, we must assume a functional form describing how the photolysis yield depends on wavelength. Both H_2O_2 and CH_3OOH gas phase quantum yields and the H_2O_2 aqueous quantum yield are constant over the atmospheric range of wavelengths.^{19,31} Therefore, we assume that the photolysis yield is independent of wavelength and use an effective wavelength-averaged photolysis yield, Φ [molecules/photon], in our calculations. The photolysis rate, J , is related to the yield by the following expression:¹²

$$J = \Phi \int \sigma(\lambda)D(\lambda)d\lambda \quad (1)$$

where σ is the (base-e) absorption cross-section [area \times molecule⁻¹] as a function of wavelength [length], λ , and $D(\lambda)$ is the radiation flux density [photons \times volume⁻¹ \times time⁻¹]. Note that we quantify the photolysis yield by measuring the number of molecules of reactant that are removed from the solution per each absorbed photon. Therefore, Φ includes contributions from the primary dissociation of CH_3OOH as well as secondary reactions. We have chosen to use hydrogen peroxide, a peroxide with similar photophysics and a known photolysis yield,³¹ to determine the photolysis yield of methyl peroxide. This relative rate approach is governed by

$$\frac{J_{\text{CH}_3\text{OOH}}}{J_{\text{HOOH}}} = \frac{\Phi_{\text{CH}_3\text{OOH}} \int \sigma_{\text{CH}_3\text{OOH}}(\lambda)D(\lambda)d\lambda}{\Phi_{\text{HOOH}} \int \sigma_{\text{HOOH}}(\lambda)D(\lambda)d\lambda} \quad (2)$$

For simplicity, we define the dimensionless constant K as

$$K \equiv \frac{\int \epsilon_{\text{CH}_3\text{OOH}}(\lambda)F(\lambda)d\lambda}{\int \epsilon_{\text{HOOH}}(\lambda)F(\lambda)d\lambda} \quad (3)$$

We can freely shift between (base-e) absorption cross-sections, σ , and the more conventional (base-10) extinction coefficients, ϵ [area \times mole⁻¹], because we can factor out and cancel the conversion factor. The extinction coefficients are determined from UV-vis absorption spectra of solutions of H_2O_2 and CH_3OOH with known concentrations. The dimensionless relative spectral density, $F(\lambda)$, is proportional to the radiation flux density. This proportionality constant, a function of the power of the lamp and geometry of the beam, can also be factored out of the integrand and canceled in cases where these factors remain constant.

Inserting the definition of the photolysis rate into eq 2 yields

$$\frac{\dot{C}_{\text{CH}_3\text{OOH}}C_{\text{HOOH}}}{\dot{C}_{\text{HOOH}}C_{\text{CH}_3\text{OOH}}} = K \frac{\Phi_{\text{CH}_3\text{OOH}}}{\Phi_{\text{HOOH}}} \quad (4)$$

where \dot{C} is the change in concentration per time [moles \times volume $^{-1} \times$ time $^{-1}$]. We choose to evaluate the photolysis rates at the start of photolysis (time = 0) to minimize the interference from absorbing products in the case of CH_3OOH (see Supporting Information). Using the Beer–Lambert law, we can transform eq 4 such that it is a function of absorbance, A , a value that we can directly measure with a UV–vis spectrometer.

$$\Phi_{\text{CH}_3\text{OOH}} = \frac{\Phi_{\text{HOOH}}}{K} \times \left(\frac{d \ln(A_{\text{CH}_3\text{OOH}})}{dt} \right)_{t=0}^{-1} \times \left(\frac{d \ln(A_{\text{HOOH}})}{dt} \right)_{t=0} \quad (5)$$

We use the expression relating the photolysis yield of H_2O_2 to temperature, T , developed by Chu and Anastasio³¹

$$\Phi_{\text{HOOH}}(T) = \frac{1}{2} \exp\left((-684 \pm 17) \left(\frac{1}{T} \right) + 2.27 \pm 0.064 \right) \quad (6)$$

The additional factor of 1/2 is needed to define the photolysis yield relative to the disappearance of reactant as opposed to the formation of product.

Experimental Procedures. To account for slow drifts of the Xenon arc lamp intensity, all measurements of CH_3OOH were done immediately before and after identical measurements for H_2O_2 . After setting the desired temperature, CH_3OOH was photolyzed for a fixed period of time by opening the lamp shutter (1 min intervals for the frozen CH_3OOH and 4 min intervals for the liquid CH_3OOH solutions). Absorption spectra were measured after each exposure (they could not be measured during photolysis because of the scattered light from the photolysis lamp). This procedure was repeated for a reference solution of H_2O_2 with a similar optical density and then followed by another measurement of a fresh CH_3OOH solution. The change in absorbance as a function of time was calculated from a weighted linear regression where points closer to $t = 0$ were assigned larger weights (for 4 successive absorption measurements, weight = 5 – N , where N is the measurement number). Linear regressions of absorption as a function of time were calculated over the series of wavelengths (240–260 nm) that had the best signal-to-noise ratio. dA/dt values from the first CH_3OOH photolysis were averaged over all applicable wavelengths and then averaged with the identical experiment performed after H_2O_2 photolysis. Equation 5, along with the photolysis yield of H_2O_2 from eq 6, were used to calculate the photolysis yield of CH_3OOH . To confirm the reproducibility, this procedure was repeated twice for each selected temperature.

Product Identification. Since we expect formaldehyde to be the dominant product of methyl peroxide photolysis, we performed a test using 2,4-dinitrophenylhydrazine (DNPH) to determine the total carbonyl concentration of the photolyzed solutions. We followed the procedure outlined in ASTM E411-

00.³² An aqueous solution of CH_3OOH , photolyzed until its absorption spectra remained constant, was reacted with an acidic DNPH solution to form the corresponding hydrazone. After neutralizing the hydrazone solution with potassium hydroxide, a deep red color develops. The absorbance at 480 nm is proportional to the concentration of carbonyl groups in solution; we used several different 2-butanone solutions to calibrate the method. The test revealed evidence of formaldehyde in the photolyzed solution but complex secondary aqueous chemistry, which can lead to hydrated gem-diols and oligomers,³³ did not allow for a quantitative measurement of its yield.

Computational Methods. The initial structures for CH_3OOH immersed in 20 water molecules were built with Avogadro,³⁴ an advanced molecule builder and visualizer. After optimization by the MMFF94 force field in Avogadro, these structures were fully optimized with MP2 in conjunction with the resolution-of-the-identity (RI) approximation³⁵ for the evaluation of the electron-repulsion integrals implemented in Turbomole.³⁶ Excitation energies were calculated by the ADC(2) method,³⁷ and the cc-pVDZ basis set³⁸ was employed. The possible structures vary due to the possible arrangement of the peroxide relative to the surface (peroxide immersed totally in the cluster versus CH_3 or OH group protruding out of the cluster). In the lowest energy structure, the CH_3 group is protruding out, while the rest of the molecule is hydrogen-bonded to the surrounding water molecules. The search for the global minimum is not possible since the cluster size is too large; thousands of local minima with comparable energies exist.

Calculations of excitation spectra were done with the semiempirical MNDO program.³⁹ The orthogonalization-corrected OM2 Hamiltonian⁴⁰ was employed to calculate the required energies and gradients. The excitation energies were obtained using the GUGA-CI approach,⁴¹ three reference configurations were used, closed shell and single and double HOMO–LUMO excitations, and the active space was chosen to include the highest six occupied orbitals and the lowest six unoccupied orbitals with twelve electrons in twelve orbitals for the isolated methyl peroxide. For the solvated methyl peroxide, the highest five occupied and unoccupied orbitals with ten electrons in ten orbitals were chosen. The active space for the isolated molecule was calibrated by comparison to the orbital excitations in ADC(2) calculations. The molecular dynamics simulations were conducted on the OM2 potential energy surface for 10 ps at three different temperatures: 50, 200, and 220 K. The time step for all simulations was 0.1 fs. One thousand structures were extracted (one structure every 10 fs of the simulation), and their vertical excitation energies and oscillator strengths were calculated with the OM2/GUGA-CI Hamiltonian. For each excitation energy, a Lorentzian (with width of 0.001 eV used for smoothing) was added. All of the Lorentzians were summed up to yield the excitation spectrum.

RESULTS

Experimental Results. The extinction coefficients of methyl peroxide in liquid and frozen water are presented in Figure 2.

Extinction coefficients in liquid water are not strongly dependent on temperature between 0 and 40 °C (see Supporting Information). They also did not change between the liquid and ice phase solutions. The absorption of CH_3OOH decreased upon freezing due to differences in scattering

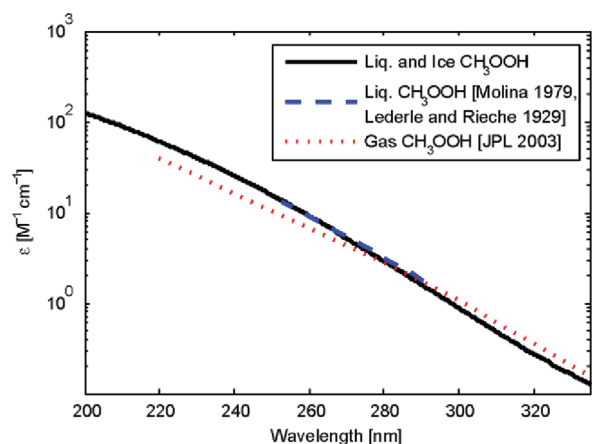


Figure 2. Comparison of CH_3OOH base-10 extinction coefficients in the gaseous,^{14,23} liquid aqueous,¹⁹ and frozen aqueous state.

between the frozen CH_3OOH solution and frozen water reference, but the spectrum maintained its shape and did not shift to the red or the blue. We find that the liquid and ice phase extinction coefficients differ from the gas phase data acquired from the JPL recommendations¹⁹ but do agree with the limited liquid phase data from Molina and Arguello¹⁴ and Lederle and Rieche.²³ In the near-UV range ($\lambda > 300$ nm), which controls tropospheric photochemistry, the gas phase extinction coefficients are larger. Between 200 and 330 nm, extinction coefficients for CH_3OOH in liquid water and ice are modeled by the following empirical equation:

$$\log_{10} \varepsilon(\lambda) = 4.9669 \times 10^{-7}(\lambda^3) - 4.3948 \times 10^{-4}(\lambda^2) + 0.1040(\lambda) - 5.1110 \quad (7)$$

where λ is in units of nm, and ε is in units of $\text{M}^{-1} \text{cm}^{-1}$. Between 200 and 290 nm, this correlation predicts the extinction coefficients within 5% error. The noise inherent in measurements of very small numbers at wavelengths between 290 and 330 nm leads to errors of up to 25%. For convenience, measured extinction coefficients are tabulated in the Supporting Information.

Figure 3 shows how the absorbance spectra of methyl peroxide (panels A and B) and hydrogen peroxide (panels C and D) evolve in the presence of actinic radiation in the liquid phase.

The absorbance of the CH_3OOH solution at 220 nm decays exponentially and reaches a steady asymptote after 150 min of photolysis. The spectrum of the final products differs in shape from the initial spectrum. Fortunately, the absorbance by the photolysis product does not exceed 10% of the initial CH_3OOH absorbance (see Supporting Information). Therefore, errors in dA/dt due to product absorption are small, especially during the early stages of an experiment, and are well within experimental uncertainties. CH_3OOH photolysis behavior can be contrasted with H_2O_2 photolysis, shown in Figure 3D. H_2O_2 photolysis does not produce absorbing products, and the absorbance decreases exponentially and completely disappears at long photolysis times. In addition, the shapes of the spectra do not change; a constant factor can transform every subsequent spectrum into the original H_2O_2 spectrum.

The results of experiments designed to measure the rate of photolysis of CH_3OOH relative to H_2O_2 are shown in Figure 4. Each data point represents the average value of two

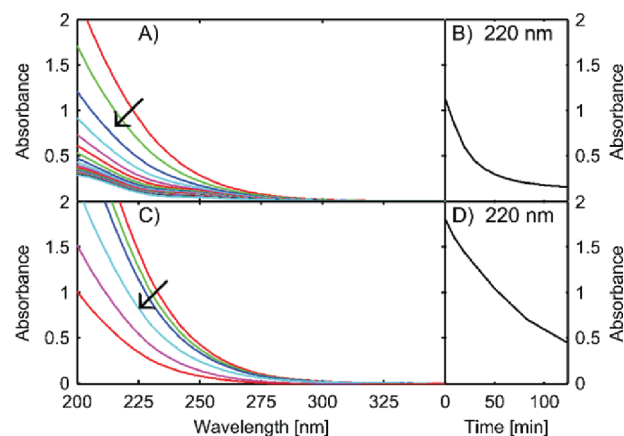


Figure 3. (A) Change in absorbance upon photolysis for a dilute aqueous solution of methyl peroxide. The direction of the arrow indicates increasing photolysis time. (B) The absorbance of the aqueous CH_3OOH solution at 220 nm as a function of time. (C) Change in absorbance of a dilute aqueous solution of hydrogen peroxide under UV light. The direction of the arrow indicates increasing photolysis time. (D) The absorbance of the aqueous H_2O_2 solution at 220 nm as a function of photolysis time.

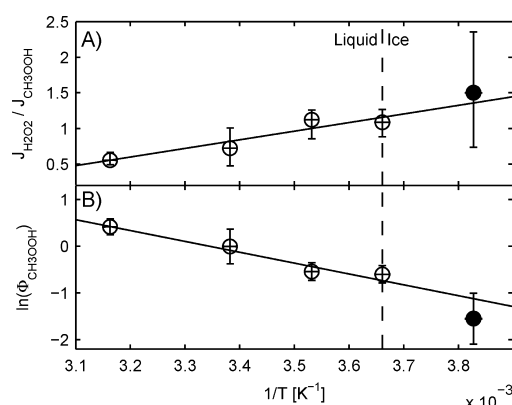


Figure 4. (A) Ratio of photolysis rate constants for CH_3OOH and H_2O_2 as a function of temperature in both the liquid and ice phase. (B) CH_3OOH photolysis quantum yield as a function of temperature. Open circles indicate that the experiment was performed with the apparatus detailed in Figure 1A. Data presented as closed circles were obtained with the apparatus shown in Figure 1B.

experiments where the photolysis rate of CH_3OOH , H_2O_2 , and CH_3OOH are measured in succession. Figure 4A displays how the relative rates of photolysis change with temperature.

Horizontal error bars are the result of uncertainties in measuring the exact temperature of the solution being photolyzed and the slight variation in temperature throughout a three-part experiment. Vertical error bars originate in the variability of photolysis rates observed at different wavelengths and in different experiments. The line through the data is the result of a least-squares analysis weighted by the combination of uncertainties in the ordinate and abscissa. Figure 4B shows how the derived photolysis yield varies with temperature. As in Figure 4A, horizontal error bars are due to uncertainties in temperature measurements and the difficulty of keeping the temperature constant in successive experiments. Vertical error bars are the result of variations in photolysis yields with wavelength and uncertainties in the photolysis yields of H_2O_2 calculated by Chu and Anastasio.³¹ The line through the data is

calculated with an uncertainty weighted least-squares analysis as in Figure 4A. The best-fit equation relating the photolysis yield of CH_3OOH to temperature is

$$\Phi_{\text{CH}_3\text{OOH}}(T) = \exp\left((-2318 \pm 461)\left(\frac{1}{T}\right) + 7.7 \pm 1.6\right) \quad (8)$$

Statistically, the ice phase experiments follow the same trend as the liquid phase experiments. The large uncertainty in the ice phase experiments dampens their contribution to the weighted least-squares fit. Removing the ice phase data changes both the intercept and slope by less than 4%. However, we advise caution when extrapolating the fit to temperatures less than -12°C because potential differences in the ice phase behavior may manifest into large discrepancies between the actual photolysis yield and the best fit line.

Theoretical Results. Methyl peroxide is found in two enantiomeric forms with a substantial rotational barrier (0.33 eV at the OM2/MRCI level) slowing the interconversion. When CH_3OOH is solvated, interconversion is further hindered by both the hydrogen-bonded water molecules adjacent to the O–O bond and to the O–H bond in CH_3OOH . For a bare methyl peroxide molecule, the MP2 method predicts a COOH dihedral angle of $\sim 120^\circ$, while the OM2 Hamiltonian (implemented in the semiempirical package MNDO) predicts a dihedral angle of $\sim 90^\circ$. When CH_3OOH is solvated in water, both methods predict a dihedral angle of $\sim 90^\circ$. A cut through the OM2 potential energy surface (PES) of the bare methyl peroxide along the dihedral angle coordinate is shown in Figure 5A (the symmetric PES of this enantiomer, which occupies COOH dihedral angles of -180° to 0° , has been omitted for simplicity).

The first excited state energy (S_1) changes significantly across the range of dihedral angles between 0° and 180° . In contrast, the ground state surface is less sensitive to the torsion around the O–O bond. There is a strong correlation between the vertical excitation energy (S_1-S_0) and the dihedral angle; specifically, the excitation energy is reduced when the molecule explores dihedral angles deviating from the minimal energy structure (90°). Even a small change in the dihedral angle gives rise to a large change in the excitation energy, for example, it is increased from 2.4 to 2.8 eV when the molecule distorts from $\phi = 90^\circ$ to $\phi = 120^\circ$. Additional details on the calculation of the vertical excitation energies with ADC(2) and OM2 are presented in the Supporting Information.

We expect the hydrated CH_3OOH to have a similar PES; however, the condensed phase should set significant constraints on the range of the dihedral angles the system can explore. A histogram detailing the distribution of the dihedral angles of the bare methyl peroxide and the hydrated methyl peroxide at 50 K is shown in Figure 5B. The bare methyl peroxide is free to explore a greater range of dihedral angles (~ 70 – 105°) than the hydrated methyl peroxide (~ 70 – 95°). The dihedral angle in the solvated methyl peroxide is more restricted because the water molecules hydrogen-bonded to the CH_3OOH molecule hinder torsion around the O–O bond. The shapes of the predicted spectra can be correlated to the distributions of COOH angles in these two cases.

We ran molecular dynamics simulations of the bare methyl peroxide and the solvated methyl peroxide for 10 ps with a time

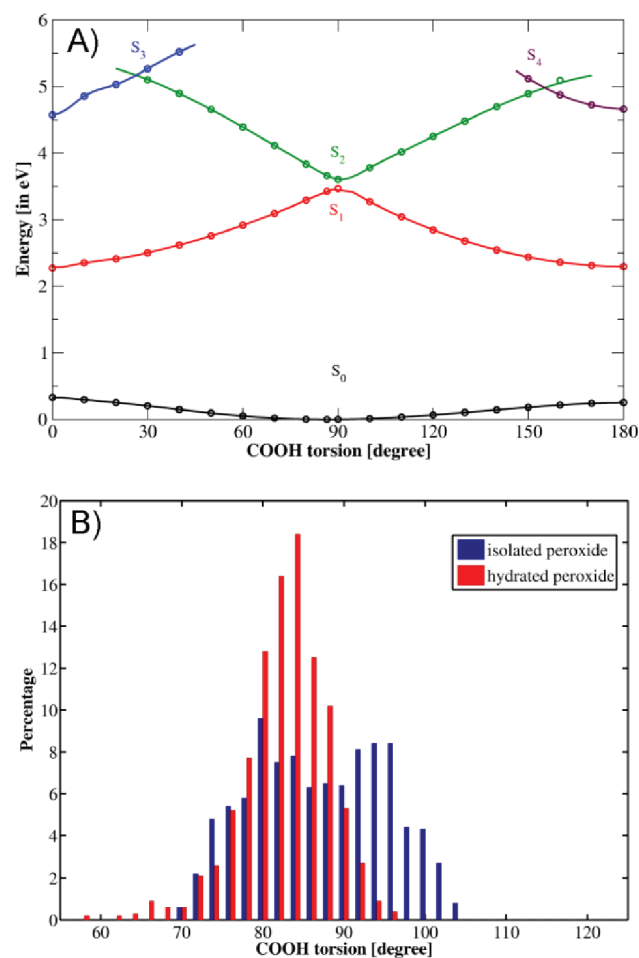


Figure 5. (A) Ground state and excited state energies as a function of the COOH dihedral angle. Only one enantiomer is shown. A symmetric potential energy surface for the other enantiomer appears between -180° and 0° . (B) Histograms showing the distribution of dihedral angles of the isolated and hydrated methyl peroxide at 50 K.

step of 0.1 fs with velocity rescaling every 20 steps to maintain a constant temperature. The excitation energy and the oscillator strength of the transition were calculated at every step. Lorentzians (with width of 0.001 eV) at each excitation energy were summed to yield the excitation spectrum. Figure 6A–C shows the excitation spectra of bare CH_3OOH compared to the excitation spectra of methyl peroxide solvated in 20 water molecules at 50K, 200K, and 220 K, respectively.

The x axis denotes the spectral shift relative to the vertical excitation energy of the bare CH_3OOH in the minimal energy geometry (90° dihedral angle). The spectral shift calculated with the OM2 Hamiltonian is comparable to the one predicted with the ADC(2) calculations; however, the absolute values differ. At 50 K, hydration of CH_3OOH shifts the whole spectrum by 0.5 eV to higher energy, representing a very large blue shift. The MD dynamic snapshots shown in Figure 6A exhibit limited changes in the CH_3OOH geometry throughout the simulation suggesting that at 50K, besides normal vibrational motion, the whole cluster and the embedded CH_3OOH molecule are extremely rigid. At 200 K (Figure 6B), the spectrum of the solvated peroxide is much more similar to the spectrum of the isolated molecule. The structure of the cluster is more flexible at 200 K; therefore, the solvated CH_3OOH is much less constrained in the dihedral angle, and in

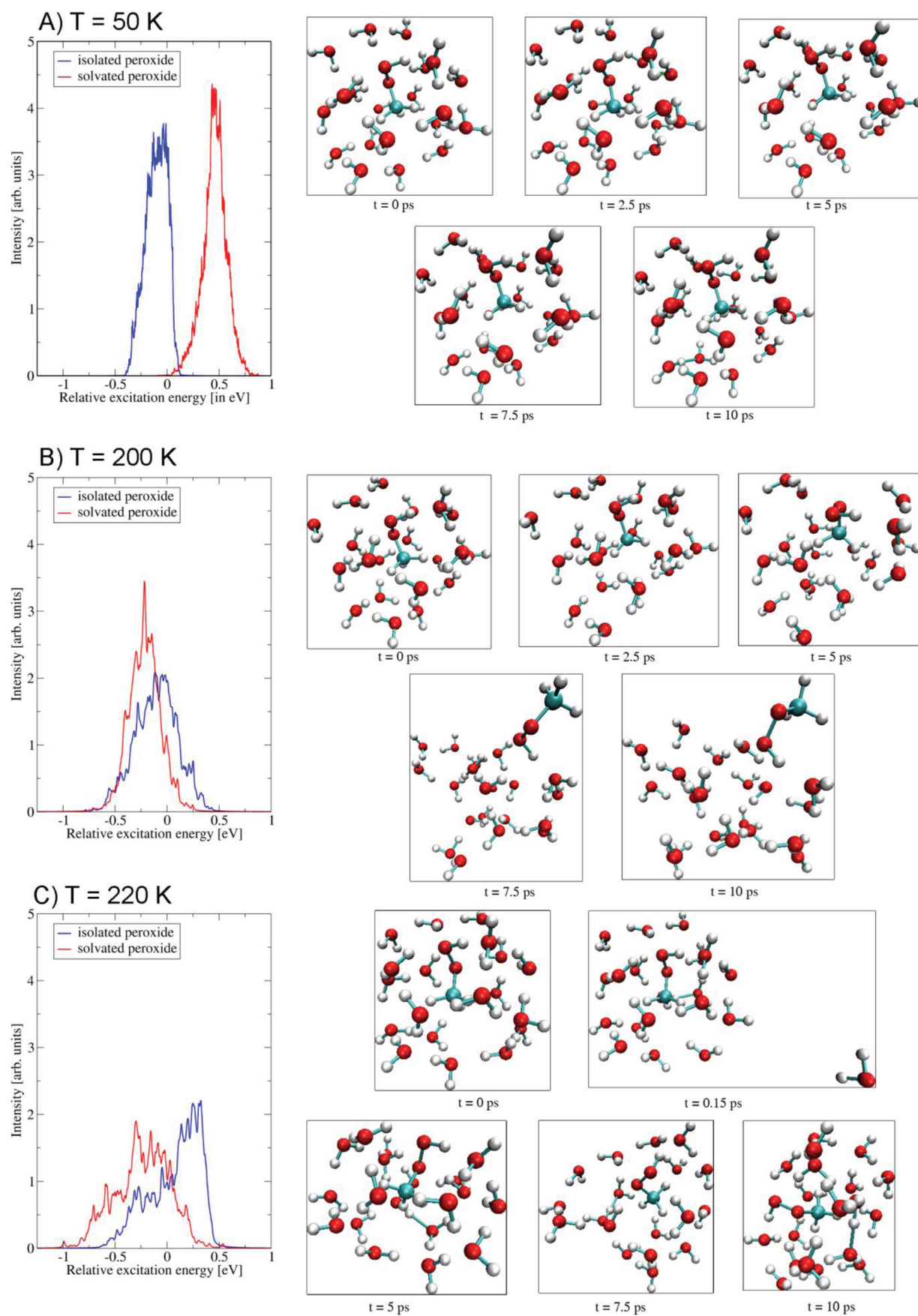


Figure 6. Computed excitation spectra of bare and solvated methyl peroxide at (A) 50 K, (B) 200 K, and (C) 220 K along with molecular dynamic snapshots. The methyl groups are shown in teal.

other motions. The fact that the peroxide attempts to evaporate after 5 ps of simulation time supports this conclusion. Comparison of panels A and B in Figure 6 clearly shows that temperature affects the spectrum of the solvated peroxide to a much greater extent compared to that in the gas phase. The calculated spectra of the solvated and bare peroxide are similar at the low energy tail. These results qualitatively agree with the experimentally measured absorption spectra of the liquid aqueous and gaseous peroxide.¹⁹ Calculations at 50 K are too cold to accurately model the experimental spectrum. The MD simulations at 220 K exhibit liquid-like behavior despite being significantly below the melting temperature of water. The binding energy predicted by OM2 is lower than the real binding energy, and therefore, the cluster melts at a lower temperature. Some water evaporation occurs, as seen in Figure 6C, at $t = 0.15$ ps. Therefore, the spectrum is broader at 220 K than the other spectra at lower temperatures.

DISCUSSION

Measured extinction coefficients of aqueous liquid and frozen methyl peroxide solutions differ from gas phase measurements. The extinction coefficients are larger in the condensed phase for $\lambda < 280$ nm and smaller at $\lambda > 280$. Placing CH_3OOH in an aqueous environment likely distorts the shapes of the lower and/or upper potential energy surfaces involved in the $n \rightarrow \sigma^*$ transition. This effect makes aqueous CH_3OOH harder to photolyze under tropospheric conditions, where the solar flux is dominated by $\lambda > 300$ nm photons. Once CH_3OOH is in the solution, its absorption spectrum does not strongly depend on temperature. Even upon freezing the solution, there are no drastic changes in the spectral or photolysis behavior. In contrast, a very large effect of freezing is predicted by the quantum calculations, with dramatic blue shift predicted at cryogenic (50 K) temperature (Figure 6). One of the questions central to our interpretation of these observations is whether the peroxide is actually frozen inside the ice or gets expelled out of the growing ice upon freezing and remains in a liquid confined between individual ice crystals. A phase diagram describing solutions of water and CH_3OOH is not available in the literature, but we can infer general trends in solution behavior from the hydrogen peroxide–water phase diagram.⁴² Even in dilute solutions, H_2O_2 remains in the liquid phase down to temperatures of -50 °C. The ice prepared from dilute H_2O_2 solutions thus represents a two-phase system with solid water and a liquid water–peroxide solution. Hydrogen bonding is suppressed in CH_3OOH relative to H_2O_2 , and therefore, we expect it to freeze at an even lower temperature than H_2O_2 in dilute solutions. Therefore, CH_3OOH most likely remains in the liquid phase at -11.8 °C, the temperature of our coldest photolysis yield experiments. This explains the lack of the temperature dependence of the extinction coefficients, as well as the lack of discontinuities in the temperature dependence of the photolysis yield between water and ice measurements.

There is evidence that reaction kinetics could change when reactant species are pushed out of water and concentrated upon freezing.⁴³ This is a concern for peroxides because the spectrum of H_2O_2 is known to blue-shift at very high concentrations.⁴⁴ However, we do not detect a change in the extinction coefficients or photolysis yields within our experimental uncertainty suggesting that such concentration effects are not significant under the present experimental conditions.

Beine and Anastasio⁴⁵ found that experiments with flash-frozen aqueous solutions of hydrogen peroxide produced

photolysis yields up to 50% smaller than previous experiments where the solutions were frozen over the course of minutes. They contend that flash freezing keeps the hydrogen peroxide in the ice matrix making recombination reactions more favorable, while slow freezing concentrates the H_2O_2 in quasi-liquid layers. In view of these effects, our reported extinction coefficients and photolysis yields may not accurately describe the photochemical behavior of an ice structure formed by co-condensation. However, our data should describe the properties of a frozen water droplet containing CH_3OOH that has been nucleated from the liquid phase or has accumulated on an ice surface (as in the case of H_2O_2).⁴⁶

Similar to H_2O_2 ,^{31,47} the photolysis quantum yield of aqueous CH_3OOH fits an Arrhenius dependence on temperature. At temperatures greater than 28 °C, we find that the photolysis yield is in excess of unity. We attribute this to the secondary reactions of the primary photolysis products such as hydroxyl radical and HO_2 radical with additional CH_3OOH molecules. The yields reported in this article thus represent an upper limit for the actual photodissociation quantum yield. We note that in actual atmospheric waters, hydroxyl radical produced by the CH_3OOH photolysis will oxidize other organics, suppressing the rate of disappearance of CH_3OOH molecules due to photolysis.

Methyl peroxide becomes less photolabile as temperatures decrease indicating that the photolysis rate in a cold air mass will be smaller than in a warm air mass. We can use eq 1 along with the extinction coefficient of liquid CH_3OOH , the photolysis yield, and the spectral actinic flux,⁴⁸ $D(\lambda)$, to calculate the expected lifetime of a CH_3OOH molecule with respect to photolysis in a water droplet. At latitudes with a solar zenith angle (SZA) of 10° such as Los Angeles in the summer, the photolysis lifetime of CH_3OOH is ~ 27 h at 32 °C and ~ 65 h at 0 °C. Higher latitudes tend to have higher SZAs and lower spectral actinic flux, which will increase the lifetime. This temperature effect has implications on both the disappearance of CH_3OOH and the subsequent chemistry inside the water droplets and ice crystals.

It is also instructive to compare the overall loss rate of CH_3OOH due to photolysis in the vapor phase and the aqueous phase under gas–water solubility equilibrium conditions. For a cloud with a liquid water content (LWC) of 3 g m^{-3} , typically the highest value found in the atmosphere,⁴⁹ we can use the temperature dependent Henry's law constant of CH_3OOH from the recommendations of the NASA/JPL panel for data evaluation¹⁹ to determine the upper limit for the rate of gaseous photolysis relative to the rate of aqueous photolysis. We used aqueous photolysis yields and extinction coefficients from this work. The gas phase photolysis yield was assumed to be equal to unity as found in several previous publications.^{3,50,51} The NASA/JPL recommendations¹⁹ were used for the gas phase absorption cross-sections. Actinic fluxes were predicted for a range of solar zenith angles on the spring equinox with the NCAR/ACD Tropospheric Ultraviolet and Visible (TUV) Radiation Model.⁴⁸ Calculations were done at sea level with an overhead ozone column of 300 Dobson units and a surface albedo of 0.1. The effect of the cloud on the solar flux was not considered, so the results are necessarily approximate. Figure 7 presents the results of this analysis.

The gas phase photolysis dominates the loss of CH_3OOH under all conditions. However, the aqueous phase photochemistry becomes more competitive with the gas phase photolysis at higher solar zenith angles and lower temperatures.

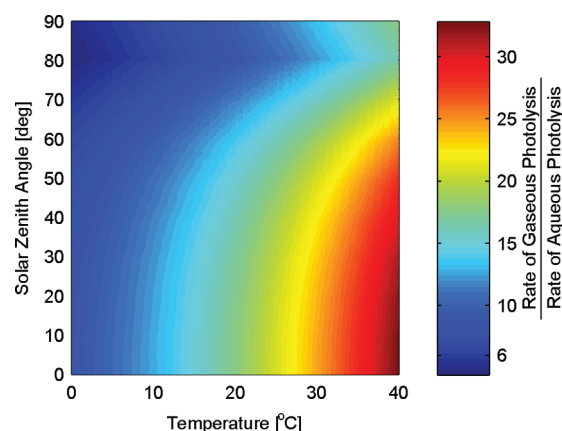


Figure 7. Relative importance of CH_3OOH aqueous photolysis to gaseous photolysis as a function of solar zenith angle and temperature in a cloud with a liquid water content of 3 g m^{-3} .

While the aqueous photolysis yield is smaller at low temperatures, the increased water solubility at low temperatures, reflected in a larger Henry's law constant, far outweighs this effect. Under optimal conditions, heavy clouds at low temperatures, aqueous phase photolysis of CH_3OOH is responsible for at most 20% of the total loss due to photolysis.

The potential energy surfaces used for the MD simulations provide a semiquantitative description of the adsorption spectra. However, for a reliable quantitative analysis, more realistic potentials are required. There are inherent limitations in the present model. The interaction energies for the ground state in the Franck–Condon region are too small. Therefore, the effective melting temperature of the model system is substantially lower than that of the actual experimental system. Also, the binding energy of the peroxide to the ice cluster, based on a comparison with a more elaborate method, is somewhat smaller than the probable real value. In general, clusters are less rigid than bulk systems (although this is not the case for interfacial regions). The theoretical model system, using the current methods, requires a lower melting temperature by several tens of degrees compared to the actual experimental system. In general, this is a key difficulty in trying to simulate water/ice systems and the spectroscopic behavior in particular. For the excited state, the uncertainty is even larger. However, we are not aware of methods that can describe electronic absorption spectra with a reasonable computational effort for systems of this nature and number of electrons. The method offers a semiquantitative, reasonable description of the excited state landscape in the Franck–Condon region. ADC(2), a coupled cluster method, is a much more reliable tool for the excited states. We used the method to describe the isolated molecule and a single point excited state calculation of the whole system. On this basis, the OM2 Hamiltonian provides a semiquantitative description of the excited state energy landscape and, therefore, the line-shape. Full ADC(2) calculation of the spectra treated here are extremely computationally demanding. OM2 cannot be used to obtain the vertical excitation peak on a quantitative footing; for this purpose, we calibrated the isolated molecule calculation with ADC(2). In summary, the semiempirical method we employed is quantitatively adequate for calculating the absorption line-shape and discussing properties of the excited state spectrum. It is also very computationally efficient. This method can be a useful tool for future simulations of electronic spectroscopy at

water/ice air interfaces provided that quantitative accuracy is not required.

CONCLUSIONS

Our experiments with aqueous liquid and frozen methyl peroxide provide the first photolysis yield measurements in the aqueous phase. We verify and quantify the presence of a carbonyl product (most likely formaldehyde) in the photolyzed solution. On-the-fly ab initio molecular dynamics simulations of a bare CH_3OOH molecule and a CH_3OOH molecule immersed inside 20 water molecules reveal that the absorption spectrum of CH_3OOH in frozen water should be sensitive to temperature, once CH_3OOH is frozen. With the measured extinction coefficients, which were found to be identical for the liquid and frozen solution, we can determine the rate of photolysis for a CH_3OOH solution in the presence of sunlight. The photolysis lifetime of CH_3OOH in water and ice is dependent on latitude, season, and temperature, but in some circumstances, it is fast enough to compete with other atmospheric sinks. However, removal of atmospheric CH_3OOH by gas phase photolysis dominates the aqueous photolysis loss under all conditions. This has significant implications for the mass balance of CH_3OOH and also cloudwater reactions initiated by the hydroxyl radical that can be formed by CH_3OOH photolysis.

ASSOCIATED CONTENT

Supporting Information

^1H NMR of methyl peroxide; extinction coefficients of CH_3OOH as a function of temperature; photographs of liquid and frozen aqueous CH_3OOH solutions; predicted CH_3OOH concentration with the iodometric peroxide test as a function of reaction time; table of extinction coefficients of dilute aqueous CH_3OOH ; comparison of the absorption spectra of aqueous CH_3OOH and its photolysis products; vertical excitation energies calculated with ADC(2) and OM2; and potential energy surface of CH_3OOH as calculated by OM2 and ADC(2). This material is available free of charge via the Internet at <http://pubs.acs.org>.

AUTHOR INFORMATION

Corresponding Author

*(S.A.N.) Tel: + 1-949-824-1262. Fax: + 1-949-824-8571. E-mail: nizkorod@uci.edu. (R.B.G.) Tel: +972 (0)26585732. Fax: +972 (0)26513742. E-mail: benny@fh.huji.ac.il.

ACKNOWLEDGMENTS

The work at the University of California, Irvine, was supported by National Science Foundation grants ATM-0831518 and CHE-0909227. The work at the Hebrew University was supported by the Israel Science Foundation, grant number 114/08, and D.S. was supported by the Lady Davis Fellowship.

REFERENCES

- Riedel, K.; Weller, R.; Schrems, O.; König-Langlo, G. *Atmos. Environ.* **2000**, *34*, 5225–5234.
- Jaeglé, L.; Jacob, D. J.; Wennberg, P. O.; Spivakovsky, C. M.; Hanisco, T. F.; Lanzendorf, E. J.; Hints, E. J.; Fahey, D. W.; Keim, E. R.; Proffitt, M. H.; Atlas, E. L.; Flocke, F.; Schauffler, S.; McElroy, C. T.; Midwinter, C.; Pfister, L.; Wilson, J. C. *Geophys. Res. Lett.* **1997**, *24*, 3181–3184.
- Blitz, M. A.; Heard, D. E.; Pilling, M. J. *J. Photochem. Photobiol., A* **2005**, *176*, 107–113.

- (4) Hewitt, C. N.; Kok, G. L. *J. Atmos. Chem.* **1991**, *12*, 181–194.
- (5) He, S. Z.; Chen, Z. M.; Zhang, X.; Zhao, Y.; Huang, D. M.; Zhao, J. N.; Zhu, T.; Hu, M.; Zeng, L. M. *J. Geophys. Res.* **2010**, *115*, D17307.
- (6) Hua, W.; Chen, Z. M.; Jie, C. Y.; Kondo, Y.; Hofzumahaus, A.; Takegawa, N.; Chang, C. C.; Lu, K. D.; Miyazaki, Y.; Kita, K.; Wang, H. L.; Zhang, Y. H.; Hu, M. *Atmos. Chem. Phys.* **2008**, *8*, 6755–6773.
- (7) Ignatov, S. K.; Gadzhiev, O. B.; Kulikov, M. Y.; Petrov, A. I.; Razuvaev, A. G.; Gand, M.; Feigin, A. M.; Schrems, O. *J. Phys. Chem. C* **2011**, *115*, 9081–9089.
- (8) Frey, M. M.; Hutterli, M. A.; Chen, G.; Sjostedt, S. J.; Burkhart, J. F.; Friel, D. K.; Bales, R. C. *Atmos. Chem. Phys.* **2009**, *9*, 3261–3276.
- (9) Valverde-Canossa, J.; Wierprecht, W.; Acker, K.; Moortgat, G. K. *Atmos. Environ.* **2005**, *39*, 4279–4290.
- (10) Hellpointer, E.; Gab, S. *Nature* **1989**, *337*, 631–634.
- (11) Docherty, K. S.; Wu, W.; Lim, Y. B.; Ziemann, P. *J. Environ. Sci. Technol.* **2005**, *39*, 4049–4059.
- (12) Bateman, A. P.; Nizkorodov, S. A.; Laskin, J.; Laskin, A. *Phys. Chem. Chem. Phys.* **2011**, *13*, 12199–12212.
- (13) Vaghjiani, G. L.; Ravishankara, A. R. *J. Geophys. Res.* **1989**, *94*, 3487–3492.
- (14) Molina, M. J.; Arguello, G. *Geophys. Res. Lett.* **1979**, *6*, 953–955.
- (15) Wang, C.; Chen, Z.; Xu, J. *Guang Pu Xue Yu Guang Pu Fen Xi* **2006**, *26*, 2222–2225.
- (16) Matthews, J.; Sinha, A.; Francisco, J. S. *J. Chem. Phys.* **2005**, *122*, 221101–221104.
- (17) Watts, J. D.; Francisco, J. S. *J. Chem. Phys.* **2006**, *125*, 104301–104309.
- (18) Roehl, C. M.; Marka, Z.; Fry, J. L.; Wennberg, P. O. *Atmos. Chem. Phys.* **2007**, *7*, 713–720.
- (19) Sander, S. P.; Golden, D. M.; Kurylo, M. J.; Moortgat, G. K.; Wine, P. H.; Ravishankara, A. R.; Kolb, C. E.; Molina, M. J.; Finlayson-Pitts, B. J.; Huie, R. E.; Orkin, V. L.; Friedl, R. R.; Keller-Rudek, H. *Chemical Kinetics and Photochemical Data for Use in Atmospheric Studies: Evaluation Number 15*; Jet Propulsion Laboratory, California Institute of Technology: Pasadena, CA, 2006.
- (20) Monod, A.; Chevallier, E.; Durand Jolibois, R.; Doussin, J. F.; Picquet-Varrault, B.; Carlier, P. *Atmos. Environ.* **2007**, *41*, 2412–2426.
- (21) Lee, M.; Heikes, B. G.; O'Sullivan, D. W. *Atmos. Environ.* **2000**, *34*, 3475–3494.
- (22) Jackson, A. V.; Hewitt, C. N. *Crit. Rev. Environ. Sci. Technol.* **1999**, *29*, 175–228.
- (23) Lederle, E.; Rieche, A. *Ber. Dtsch. Chem. Ges.* **1929**, *62*, 2573–2585.
- (24) Kahan, T. F.; Kwamena, N.-O. A.; Donaldson, D. J. *Atmos. Chem. Phys.* **2010**, *10*, 10917–10922.
- (25) Nguyen, T. B.; Bateman, A. P.; Bones, D. L.; Nizkorodov, S. A.; Laskin, J.; Laskin, A. *Atmos. Environ.* **2010**, *44*, 1032–1042.
- (26) Kulkarni, A. D. *J. Chem. Phys.* **2009**, *131*, 054310.
- (27) Kamboures, M. A.; Nizkorodov, S. A.; Gerber, R. B. *Proc. Natl. Acad. Sci. U.S.A.* **2010**, *107*, 6600–6604.
- (28) Shemesh, D.; Gerber, R. B. *Mol. Phys.*, submitted.
- (29) Banerjee, D. K.; Budke, C. C. *Anal. Chem.* **1964**, *36*, 792–796.
- (30) Kasha, M. *J. Opt. Soc. Am.* **1948**, *38*, 929–933.
- (31) Chu, L.; Anastasio, C. *J. Phys. Chem. A* **2005**, *109*, 6264–6271.
- (32) ASTM. E411-00, Standard Test Method for Trace Quantities of Carbonyl Compounds with 2,4-Dinitrophenylhydrazine, 2000.
- (33) Dong, S.; Dasgupta, P. K. *Environ. Sci. Technol.* **1986**, *20*, 637–640.
- (34) Avogadro: An Open-Source Molecular Builder and Visualization Tool, Version 1.0. <http://avogadro.openmolecules.net/>.
- (35) Weigend, F.; Haser, M. *Theor. Chem. Acc.* **1997**, *97*, 331–340.
- (36) Ahlrichs, R.; Bar, M.; Haser, M.; Horn, H.; Kolmel, C. *Chem. Phys. Lett.* **1989**, *162*, 165–169.
- (37) Schirmer, J. *Phys. Rev. A* **1982**, *26*, 2395–2416.
- (38) Dunning, T. H. *J. Chem. Phys.* **1989**, *90*, 1007–1023.
- (39) Thiel, W. *MNDO Program*, version 6.1; Mülheim an der Ruhr: Germany, 2007.
- (40) Weber, W.; Thiel, W. *Theor. Chem. Acc.* **2000**, *103*, 495–506.
- (41) Koslowski, A.; Beck, M. E.; Thiel, W. *J. Comput. Chem.* **2003**, *24*, 714–726.
- (42) Giguere, P. A. *Peroxyde d'hydrege et polyoxydes d'hydrogene*; Masson et Cie: Paris, France, 1975.
- (43) Takenaka, N.; Bandow, H. *J. Phys. Chem. A* **2007**, *111*, 8780–8786.
- (44) Pibbs, M. K.; Giguere, P. A. *Can. J. Chem.* **1951**, *29*, 490–493.
- (45) Beine, H.; Anastasio, C. *J. Geophys. Res.* **2011**, *116*, D14302.
- (46) Jacobi, H.-W.; Frey, M. M.; Hutterli, M. A.; Bales, R. C.; Schrems, O.; Cullen, N. J.; Steffen, K.; Koehler, C. *Atmos. Environ.* **2002**, *36*, 2619–2628.
- (47) Zellner, R.; Exner, M.; Herrmann, H. *J. Atmos. Chem.* **1990**, *10*, 411–425.
- (48) Madronich, S. TUV: Tropospheric Ultraviolet and Visible Radiation Model. <http://cprm.acd.ucar.edu/Models/TUV/index.shtml> (accessed Oct 2011).
- (49) Seinfeld, J. H.; Pandis, S. N. *Atmospheric Chemistry and Physics: From Air Pollution to Climate Change*; John Wiley & Sons, Inc.: New York, 1998.
- (50) Vaghjiani, G. *J. Chem. Phys.* **1990**, *92*, 996.
- (51) Thelen, M. A.; Felder, P.; Robert Huber, J. *Chem. Phys. Lett.* **1993**, *213*, 275–281.